Journal of Marine Research, 45, 107–131, 1987

Single-particle dispersion, Lagrangian structure function and Lagrangian energy spectrum in two-dimensional incompressible turbulence

by Armando Babiano,[1] Claude Basdevant,[1] Pascal Le Roy[1] and Robert Sadourny[1]

ABSTRACT

The single-particle dispersion, Lagrangian structure functions and Lagrangian energy spectra characteristic of two-dimensional incompressible turbulent flows are investigated theoretically *and numerically. The domain of validity of the classical asymptotic estimates is extended; it is* shown in particular that the asymptotic behavior of the single-particle dispersion at small times remains valid throughout the whole self-similar range when the Lagrangian energy spectrum is steeper than ω^{-1}. Straightforward estimates of the Lagrangian integral time scale T_L and the diffusion coefficient at large times $\mathcal{K}$, based on energy and enstrophy, are proposed; to some extent, they remain valid locally, which allows an analysis of the spatial variability of T_L and $\mathcal{K}$, within a single turbulent field. Finally, the detrimental effect of artificial numerical diffusion on the numerical simulation of Lagrangian statistics is highlighted and discussed.

1. Introduction

Flow measurements by means of Lagrangian tracers are now becoming widely used in dynamic oceanography (see for example Freeland *et al.,* 1975). The synoptic circulation and its quasi-two-dimensional regime will be studied in the near future using such Lagrangian observational techniques sustained by recent advances in buoy technology and localization devices such as the ARGOS Satellite Location and Data Collection System (1978). In relation to these developments, a number of new problems are arising. The aim of the present work is to clarify the kind of information on the macro-turbulent structure of the large-scale oceanic flow to be retrieved from drifting buoy trajectories. More precisely, our main purpose here is to investigate the variability of the eddy diffusion coefficient in a two-dimensional turbulent flow-field containing sporadic coherent vortex concentrations, considered as an elementary model of large-scale oceanic motion; the presence of coherent vortices (McWilliams, 1984; Couder *et al,* 1984) as well as nonlocality (Bennett, 1984), important consequences for particle dispersion.

First we consider the formulation and theory of Lagrangian statistics in general,

1. Laboratoire de Météorologie Dynamique du CNRS, Ecole Normale Supérieure, 24, rue Lhomond, 75231 Paris Cedex 05, France.

involving Lagrangian energy spectra and single-particle dispersion, by following closely the approach already used by Babiano *et al.* (1985b)—hereafter refered to as BBS—for Eulerian statistics. We insist on the natural relations between the Lagrangian spectrum, the single-particle dispersion and the diffusion coefficient, which lead to a consistent interpretation of asymptotic behaviors at both small and large times. The Lagrangian time scale is also investigated in terms of its relation to enstrophy; so is the asymptotic value of the diffusion coefficient, related in turn to the proper combination of energy and enstrophy.

The analysis is then followed and sustained by a set of numerical experiments, where ensembles of particles are released in selected areas of a two-dimensional turbulent flow obtained from numerical simulations of the two-dimensional Navier-Stokes equations; the launching areas are selected to provide separate investigations of Lagrangian statistics in the various conditions encountered in such a flow, from strong coherent vortices to weak turbulent surroundings. The problem of numerical diffusion and its impact on the Lagrangian statistics, is addressed.

2. Definitions and relations

We consider the time evolution of the separation of a fluid particle from its initial position in a homogeneous, stationary, zero-mean two-dimensional turbulent velocity field. The squared displacement of the particle identified by its Lagrangian coordinate **a** (its position at time $t = 0$) is given by:

$$P^2(\mathbf{a}, t) = \left(\int_0^t \mathbf{V}(\mathbf{a}, \tau) d\tau \right)^2, \tag{1}$$

which leads to

$$\frac{1}{2} \frac{d}{dt} P^2(\mathbf{a}, t) = \int_0^t \mathbf{V}(\mathbf{a}, t) \cdot \mathbf{V}(\mathbf{a}, \tau) d\tau. \tag{2}$$

Relations (1, 2) will be studied in statistical mean, using the average $\langle \cdot \rangle$ over all initial positions **a**. We define the single-particle dispersion as

$$A(t) = \langle P^2(\mathbf{a}, t) \rangle. \tag{3}$$

The coefficient of eddy diffusion is then defined by

$$K(t) = \frac{1}{2} \frac{d}{dt} A(t). \tag{4}$$

All these definitions can be generalized to tensor notation, but such generality is not needed in the present context.

a. The Lagrangian structure function. Let us recall some definitions and relations involving the second-order Lagrangian structure function. The Lagrangian structure

function is defined as

$$S_L(t) = \frac{1}{2}\langle \|\mathbf{V}(\mathbf{a}, 0) - \mathbf{V}(\mathbf{a}, t)\|^2 \rangle; \tag{5}$$

and the Lagrangian velocity correlation coefficient as

$$R_L(t) = \frac{\langle \mathbf{V}(\mathbf{a}, 0) \cdot \mathbf{V}(\mathbf{a}, t) \rangle}{\langle \|\mathbf{V}(\mathbf{a}, 0)\|^2 \rangle}. \tag{6}$$

Denoting by E the mean initial energy of the particles

$$E = \tfrac{1}{2}\langle \|\mathbf{V}(\mathbf{a}, 0)\|^2 \rangle, \tag{7}$$

which approaches the mean energy of the flow as the particle sampling gets dense enough, we may write

$$S_L(t) = 2E(1 - R_L(t)). \tag{8}$$

The asymptotic behavior of the Lagrangian structure function at small times is given by (Babiano *et al.*, 1985a)

$$S_L(t) \sim Ct^2, \qquad t \to 0 \tag{9}$$

with

$$C = \frac{\langle \|\nabla p\|^2 \rangle}{2\rho^2} \tag{10}$$

where ρ refers to density and p to pressure.

Assuming a finite Lagrangian integral time scale

$$T_L = \int_0^\infty R_L(t)\, dt \tag{11}$$

the Lagrangian structure function, at times larger than T_L, converges toward two times the energy

$$S_L(t) \sim 2E \qquad t \gg T_L. \tag{12}$$

b. The Lagrangian integral time scale. The Lagrangian integral time scale can be related to enstrophy, according to the following argument. At small times (8) and (9) yield

$$R_L(t) \sim 1 - \frac{C}{2E}t^2. \tag{13}$$

To estimate T_L, we make the classical assumption that the integral of $R_L(t)$ (11) is essentially determined by its curvature at $t = 0$. Thus we may approximate $R_L(t)$, using

(13), by the Gaussian

$$R_L(t) = \exp\left(-\frac{C}{2E}t^2\right),$$

which yields

$$T_L = \frac{1}{2}\sqrt{\frac{2\pi E}{C}}. \tag{14}$$

We now have to estimate C; for this, we may use relation (10) and Millianchikov's quasi-gaussianity hypothesis (Batchelor, 1951), which give

$$C = 6E^2 \int_0^\infty \frac{1}{r}\left(\frac{d}{dr}R_{//}(r)\right)^2 dr. \tag{15}$$

Using the same argument as above, we again approximate $R_{//}(r)$ by a Gaussian whose curvature at the origin is given by relation (5) of BBS:

$$R_{//}(r) = \exp\left(-\frac{Z}{8E}r^2\right)$$

where Z refers to enstrophy

$$Z = \tfrac{1}{2}\langle \|\text{curl } \mathbf{V}\|^2 \rangle.$$

Then (15) is readily integrated to yield

$$C = \tfrac{3}{4}EZ, \tag{16}$$

$$T_L = \sqrt{\frac{2\pi}{3}}Z^{-1/2}. \tag{17}$$

The general form of (16) and (17) could be anticipated on simple dimensional arguments; the advantage of the analytical development is that it yields numerical values for the proportionality constants, which can be verified experimentally. Further, the Lagrangian integral time scale T_L is usually interpreted as the length of time during which a particle keeps its initial direction; this time scale is thus related to the curvature of trajectories and to velocity shears, both being measured by Z. Finally, we may also point out that, Z being (in the weak dissipation limit) a Lagrangian invariant, (17) can be efficiently used for any subset of practicles in the flow domain.

c. Relations between Lagrangian structure function and single-particle dispersion. Using the above definitions one classically obtains:

$$A(t) = 4E\int_0^t R_L(\tau)(t-\tau)d\tau = 4E\int_0^t \left(1 - \frac{S_L(\tau)}{2E}\right)(t-\tau)d\tau, \tag{18}$$

$$K(t) = 2E \int_0^t R_L(\tau) d\tau = 2E \int_0^t \left(1 - \frac{S_L(\tau)}{2E}\right) d\tau. \tag{19}$$

Relations (9) and (11), added to (18) and (19), yield the following asymptotic behaviors for the single-particle dispersion:

$$\left.\begin{aligned} A(t) &\sim 2Et^2\left(1 - \frac{C}{12E}t^2\right) \\ K(t) &\sim 2Et\left(1 - \frac{C}{6E}t^2\right) \end{aligned}\right\}, \quad t \ll T_L, \tag{20}$$

$$\left.\begin{aligned} A(t) &\sim 2\mathcal{K}t \\ \mathcal{K} &\sim 2ET_L \end{aligned}\right\}, \quad t \gg T_L. \tag{21}$$

Formulas (20) (without the correction term in t^4) and (21) were given first by Taylor (1921), then by Kampé de Fériet (1939).

d. Relations with the Lagrangian spectrum. The Lagrangian energy spectrum is defined by

$$L(\omega) = \frac{2E}{\pi} \int_0^\infty R_L(t) \cos \omega t \, dt; \tag{22}$$

it is then related to the structure function by

$$S_L(t) = 4 \int_0^\infty \sin^2 \frac{\omega t}{2} L(\omega) d\omega, \tag{23}$$

and to the single-particle dispersion by:

$$A(t) = 8 \int_0^\infty \frac{\sin^2 \dfrac{\omega t}{2}}{\omega^2} L(\omega) d\omega. \tag{24}$$

The analysis of relation (24) shows (Kampé de Fériet, 1939; Batchelor, 1949) that at small times all Lagrangian frequencies contribute equally to the aymptotic behavior (20) of the single-particle dispersion. Conversely, at large times, small frequencies dominate in (24), which leads to the following approximations:

$$\left.\begin{aligned} A(t) &\sim 2\pi L(0)\, t \\ \mathcal{K} &\sim \pi L(0) \end{aligned}\right\} (t \gg T_L). \tag{25}$$

Thus at large times the eddy diffusion coefficient is related to the Lagrangian energy at the smallest frequencies. The implications of relations (23) and (24) on the Lagrangian

structure function and single-particle dispersion in the case of a self-similar spectrum will be discussed in the next section.

3. Behavior in a self similar range

Re-examining the relation between Eulerian energy spectra and Eulerian structure functions or relative dispersion, BBS have shown that the latter saturate at a r^2 dependency as soon as the former get steeper than k^{-3}. This implies in particular that energy spectrum is difficult to reconstruct from conventional Eulerian velocity correlation measurements alone. The arguments developed in BBS are in fact very general and can be directly restated in the Lagrangian framework involving Lagrangian energy spectra, Lagrangian structure functions and single-particle dispersion.

a. The Lagrangian structure function. For instance, either (23) or formula (22) of BBS yield the following behaviors of the Lagrangian or Eulerian structure functions according to the slope-n of the corresponding (Lagrangian or Eulerian) energy spectrum

$$\left.\begin{aligned} n < 1 \quad & dS/d\sigma \sim 0 \\ 1 < n < 3 \quad & S(\sigma) \sim \sigma^{n-1} \\ n > 3 \quad & S(\sigma) \sim \sigma^2 \end{aligned}\right\}, \tag{26}$$

where σ refers either to the spatial scale (in the Eulerian case) or to time (in the Lagrangian case). Therefore the Lagrangian structure function also saturates at a t^2 dependency for steep Lagrangian energy spectra, with the same detrimental effects as stated above on reconstructing the latter from observations. Like in the Eulerian case, the t^2 dependency extends the small-time behavior (9) to the whole inertial range; replacing C by its value (16), we get

$$S_L(t) = \tfrac{3}{4}\, EZt^2, \tag{27}$$

or in terms of E and T_L

$$S_L(t) = \frac{\pi}{4}\,(t/T_L)^2\, E. \tag{28}$$

b. The single-particle dispersion. Similarly, the arguments given in BBS, applied to relation (24), yield the following expression for single-particle dispersion

$$A(t) = 8t^{n+1} \int_{\omega_1 t}^{\omega_2 t} \sin^2 \frac{u}{2}\, u^{-(n+2)} du, \tag{29}$$

for a Lagrangian energy spectrum $L(\omega) = \omega^{-n}$ with low- and high-Lagrangian

frequency cut-offs ω_1 and ω_2. From (29) we get a relation analogous to relation (24) of BBS:

$$A(t) = t^{n+1}\left[\frac{1}{4(1-n)}(2^{(1-n)/2} - (\omega_1 t)^{1-n}) - \frac{1}{2(n+1)}((\omega_2 t)^{-(n+1)} - 2^{(n+1)/2})\right], \quad (30)$$

yielding the following behavior:

$$\left.\begin{array}{lll} \text{(i)} & n > 1 & A(t) \sim t^2 \\ \text{(ii)} & -1 < n < 1 & A(t) \sim t^{n+1} \\ \text{(iii)} & n < -1 & dA/dt \sim 0 \end{array}\right\}. \quad (31)$$

We proceed to a brief discussion of the three cases.

(i) $n > 1$. The t^2 dependency of the single-particle dispersion across the self-similar range, obtained in the nonlocal case ($n > 3$) by the analysis of the Lagrangian structure function, is now proven in a more general case ($n > 1$). This result explains the weak dependency of the single-particle dispersion upon the Lagrangian structure function shape noted by Taylor (1921) and Frenkiel (1952, 1953).

(ii) $-1 < n < 1$. Linear dependency of the single-particle dispersion upon time implies a constant energy spectrum ($n \simeq 0$). But we have seen, from relations (21) or (25), that $A(t)$ is indeed linear at large times. This means that the Langrangian energy spectrum must be white at small frequencies. It also means that the asymptotic linear behavior of $A(t)$ will be reached more or less quickly, depending whether this asymptotic flatness of the energy spectrum extends more or less to intermediate frequencies.

(iii) $n < -1$. This case, where the single-particle dispersion is constant, occurs for an increasing spectrum, for instance just after a spectral gap.

c. The diffusion coefficient. Definition (4) together with relations (31), yield the following behaviors of the diffusion coefficient:

(i) $n > 1 : K(t)$ is linear in t. In this case the asymptotic behavior at small times (20) extends throughout the whole range of time scales:

$$K(t) = 2Et, \qquad (n > 1) \quad (32)$$

(ii) $-1 < n < 1$. In this case

$$K(t) \sim t^n, \qquad (-1 < n < 1). \quad (33)$$

Table 1. Characteristic parameters of the numerical experiment.

L	1000 km	
forcing scale R	50 km	
small-scale dissipation	t_c = 6h30	ℓ_c = 7,8 km
large-scale friction	t_d = 76 days	ℓ_d = 500 km
time step	Δt = 1 h	
energy	12.5 cm^2 · s^{-2}	
enstrophy	0.0177 (day)$^{-2}$	
enstrophy dissipation rate	1.38 10^{-4} (day)$^{-3}$	

The interesting case is the case $n = 0$, which, as we have already seen, is the asymptotic case for large times. Then $K(t)$ is constant, its value being given by the asymptotic value (21):

$$K(t) = \mathcal{K} = 2ET_L, \qquad (n = 0). \tag{34}$$

Then, the estimate (17) of the Lagrangian integral time scale yields

$$\mathcal{K} = \sqrt{\frac{8\pi}{3}} EZ^{-1/2}, \qquad (n = 0). \tag{35}$$

Like in (16, 17), we have here an explicit value of the proportionality constant, which has been derived from analytical developments and can be verified on experimental grounds. A more complicated estimate, although dimensionally similar, has been proposed by Holloway and Kristmannson (1984).

(iii) $n < -1$. In this case (31) yields

$$K(t) \sim 0, \qquad (n < -1). \tag{36}$$

4. Numerical experiments

The Eulerian numerical model (Basdevant *et al.*, 1981) integrates the quasi-geostrophic barotropic vorticity equation

$$\frac{d\zeta}{dt} + J(\psi, \zeta) = F(\zeta) + G(\zeta)$$

on a doubly periodic square domain of side L, using a pseudo-spectral approximation on a 128 × 128 grid. Here ψ refers to the stream-function, ζ to vorticity; $F(\zeta)$ and $G(\zeta)$ respectively to the forcing and dissipation term. Dissipation is defined as

$$G(\zeta) = -t_c^{-1}(-\ell_c^2\Delta)^8\zeta + t_d^{-1}\ell_d^{-2}\psi$$

where t_c and t_d are characteristic times, and ℓ_c the cutoff scale and ℓ_d the largest scale. Dissipation thus involves a "super-viscosity" based on an iterated Laplacian (Basdevant *et al.*, 1983), designed to dissipate essentially enstrophy near the cutoff scale, and

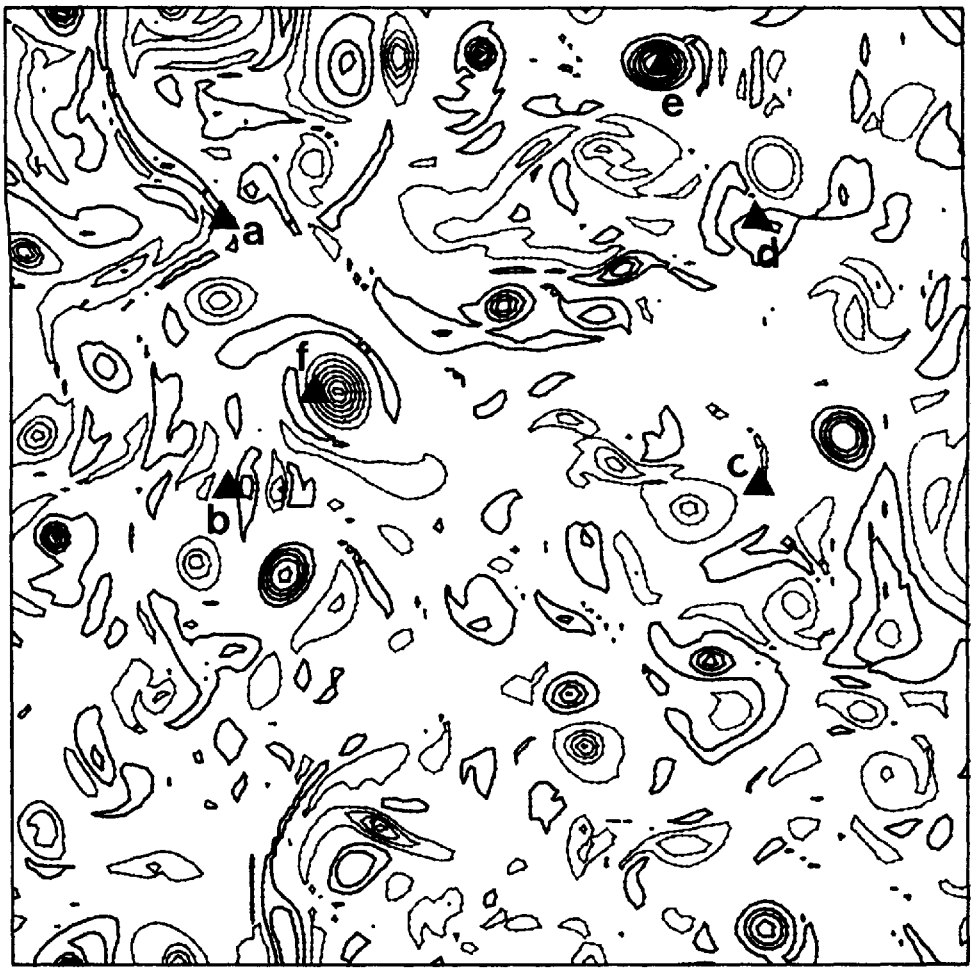

Figure 1. Initial vorticity field and localization of the six sets of tracers (a to f).

a linear "friction" designed to dissipate energy at larger scales. Forcing is included by keeping the amplitude of the zonal mode $k_1 = (0, 10)$ constant in time.

The model is integrated until stationary regime conditions are reached. At that stage, the characteristic parameters of the flow are thos listed in Table 1.

At this stage particles are released in the flow and their Lagrangian motion is obtained by integrating their transport equation using a first-order forward scheme with a time step τ

$$\mathbf{x}(t + \tau) = \mathbf{x}(t) + \tau \mathbf{V}(\mathbf{x}(t), t).$$

The velocity $\mathbf{V}$ at $\mathbf{x}(t)$ is evaluated by linear interpolation within the relevant mesh. All

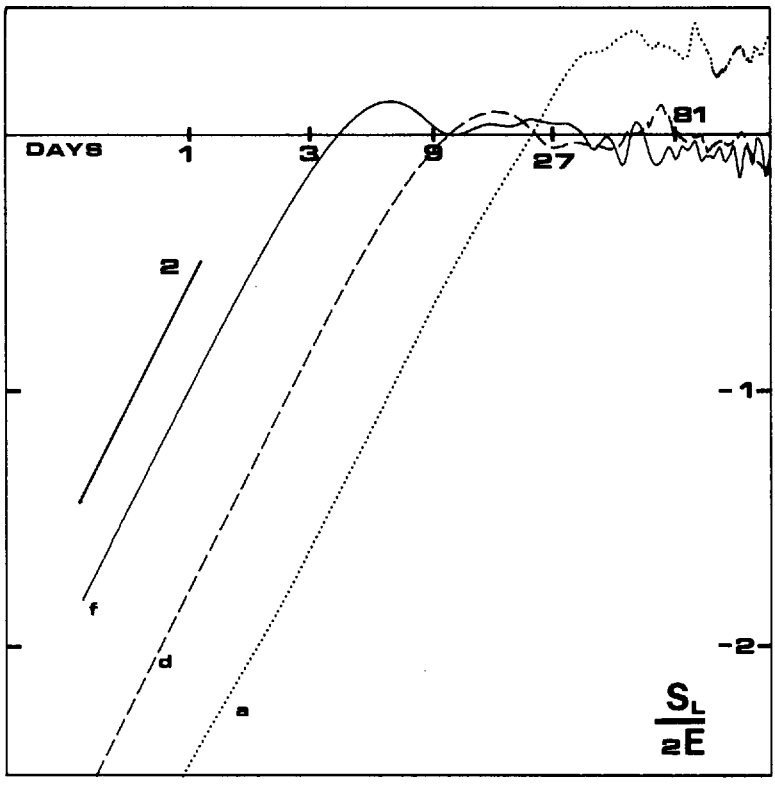

Figure 2. Lagrangian structure functions as a function of time for particle sets a, d and f (log-log scale); the t^2 dependency is indicated.

experiments described in this paper use a time step τ equal to the time step Δt used for integrating the equation of motion (which therefore verifies the CFL criterion).

The statistics leading to evaluation of Lagrangian structure functions, spectra, correlations and integral time scales, as well as the evaluation of absolute dispersion and large-scale diffusion coefficients, are constructed by following a set of fourteen initially square patches of 10 × 10 particles released at contiguous gridpoints in selected areas of the flow (Fig. 1). We first proceed to a detailed account of the results; the question of how much they are affected by spurious numerical diffusion will be addressed in Section 5.

a. Lagrangian structure functions. The Lagrangian structure functions computed separately for patches a, d, f of Figure 1 are displayed in Figure 2. These three patches have been chosen because they correspond to distinct energy or enstrophy levels: a is a weakly energetic area, f is strongly energetic, and d corresponds to the average energy of the flow (see Table 2 for more quantitative details). We indeed observe a t^2 behavior

Table 2. Adimensional measures of energy E, enstrophy Z, Lagrangian time scale T_L, and combinations thereof within 14 patches labeled from a to n. The length scale and time scale used for adimensionalization are $l_* = 159.1$ km and $t_* = 386.3$ days.

	E	Z	T_L	$2ET_L$	$EZ^{-1/2}$
a	14.86	1838.7	0.052	1.55	0.35
b	25.28	2364.2	0.056	2.83	0.52
c	65.66	497.3	0.038	4.99	2.94
d	65.43	5596.7	0.0158	2.067	0.87
e	239.3	23167	0.0075	3.59	1.57
f	319.9	31460	0.0057	3.64	1.8
g	17.19	1254	0.0555	1.9	0.48
h	9.22	299	0.0895	1.65	0.53
i	111.21	6493.8	0.015	3.33	1.38
j	181.7	15123	0.00925	3.36	1.48
k	195.0	18417.3	0.007	2.73	1.44
l	15.25	1223	0.043	1.31	0.44
m	108	10983.7	0.00925	2	1.03
n	24.2	2570	0.0215	1.04	0.48

at small times, which in all three cases, extends approximately to the corresponding T_L (see again Table 2). The three structure functions can be used to quantitatively verify relation (27). In (27), the coefficient $\frac{3}{4}EZ$ has been obtained from asymptotic arguments at small times; therefore, here E and Z have to be taken as the initial value of energy and enstrophy in each patch. In doing this we obtain, instead of the value $\frac{3}{4}$ predicted by (27): .54 for patch a, .89 for patch d and .96 for patch f. For $t > T_L$, $S_L(t)$ is practically constant. There is no visible transition range between the two regimes.

b. Lagrangian energy spectra. Two distinct regimes are also seen on the Lagrangian energy spectra (Fig. 3); they are approximately separated by T_L^{-1} and are consistent with the two regimes of $S_L(t)$.

At high frequencies ($\omega > T_L^{-1}$), $L(\omega)$ is steeper than ω^{-3} as expected; more precisely, $L(\omega)$ is significantly steeper than ω^{-3} for frequencies slightly higher than T_L^{-1}; but at very high frequencies ($\omega \gg T_L^{-1}$), all spectra saturate at ω^{-3}. This clearly illustrates *the systematic bias encountered in reconstructing an energy spectrum from a set of* correlation measurements, already mentioned in BBS for Eulerian spectra. The correlation technique, if based upon an insufficient amount of data, tends to yield the noisiest spectrum compatible with the t^2 correlation law; i.e., a ω^{-3} spectrum. A precise estimate of the real slope, if it is steeper than ω^{-3}, would require an unrealistically large number of tracers. Figure 4 shows two estimates of the Lagrangian energy spectrum over the whole domain of the flow, using either 256 or 4096 tracers; the -3 law disappears in the second case.

At low frequencies ($\omega < T_L^{-1}$), we expect flat spectra, in accordance with (26) and

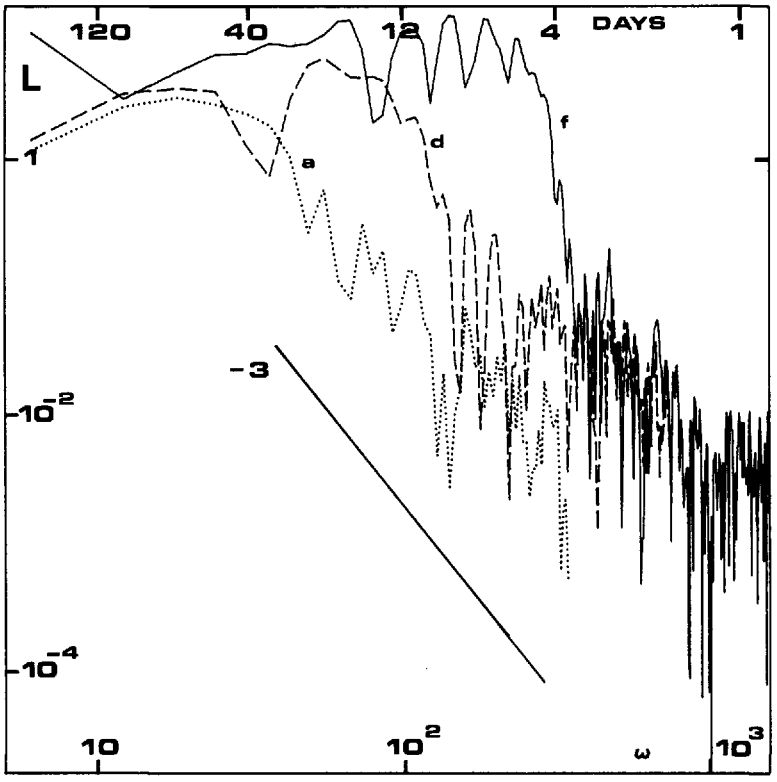

Figure 3. Lagrangian energy spectra of particle sets a, d and f (log-log scale); the ω^{-3} dependency is indicated.

the constant structure functions already found in Figure 2. In turn, this behavior indicates, from (31), a linear behavior of $A(t)$, or in other words, a constant dispersion coefficient given by (34).

c. Lagrangian correlations and integral scales. We show in Figure 5 the Lagrangian correlations $R_L(t)$ obtained for the six patches of Figure 1, and in Figure 6, the corresponding values of T_L computed from (11), in relation to the local estimates of Z or E given in Table 2. The diagram (T_L, E) of Figure 6b yields an estimate of the variability of the dispersion coefficient $\mathcal{K}$, as deduced from formula (21); the extreme values of $\mathcal{K}$ are within a factor 5, in spite of the large range of energies and enstrophies involved in the choice of our patches (energy varies up to a factor 35 while enstrophy varies up to a factor 100). Simultaneous estimates of E and $\mathcal{K}$ reported from observations in the ocean (Freeland *et al.*, 1975; Price, 1981; Colin de Verdiere, 1983) are also plotted in Figure 6b. Figure 6a shows that T_L closely follows the $Z^{-1/2}$

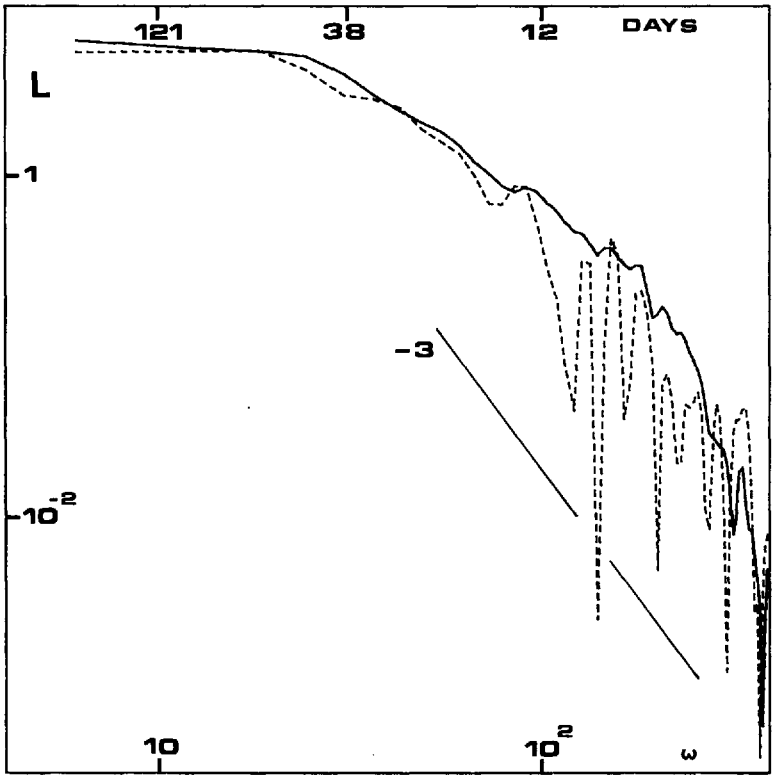

Figure 4. Lagrangian energy spectrum of the whole flow. Solid line: estimation using 4096 particles. Dotted line: degraded estimation using 256 particles (log-log scale). The ω^{-3} dependency is indicated.

dependency predicted by relation (17), especially in coherent vortex areas; the coefficient $\sqrt{2\pi/3}$, however, appears overestimated; the experimental value is around 1.12 rather than 1.45. There is, to our knowledge, no observation of Z in the ocean, connected with either measurements of the dispersion coefficient, or measurements of T_L.

d. Single-particle dispersion. The dispersion coefficient $\mathcal{K}$ is given in Figure 7a as a function of $EZ^{-1/2}$, according to formula (35). The formula is again reasonably verified, but again it overestimates the slope by a factor 1.3. $\mathcal{K}$ appears less well correlated to E than it is to $EZ^{-1/2}$, as shown by Figure 7b.

The absolute dispersion $A(t)$ is shown on Figure 8, again for patches a to f. We verify that the asymptotic law $A(t) \sim t^2$ extends indeed to time scales of the order of T_L, as expected from (31) or (20); moreover, the coefficient $2E$ predicted by (20) is in

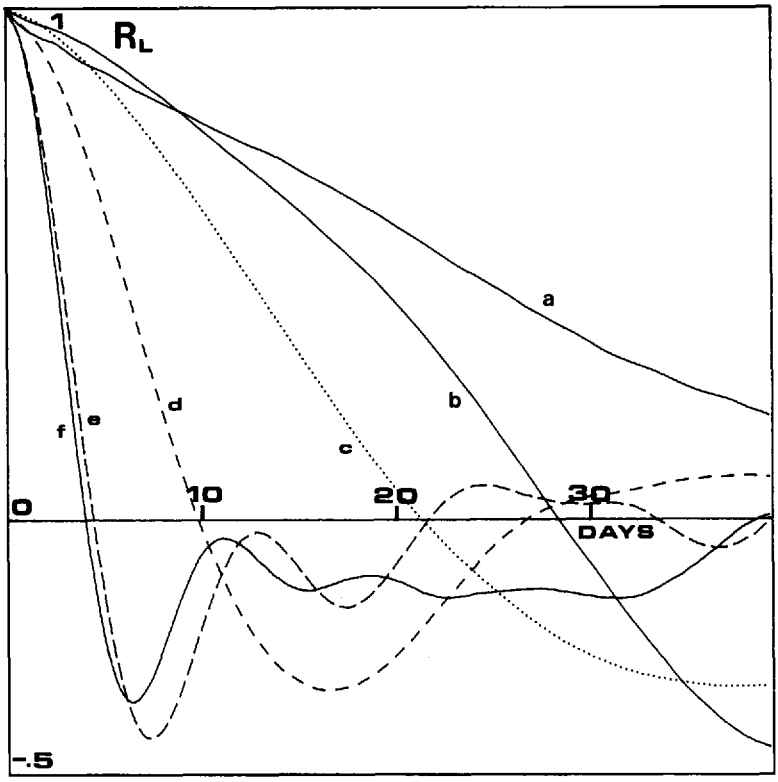

Figure 5. Lagrangian velocity correlations $R_L(t)$ for particle sets a to f.

excellent accordance with the numerical simulations. At $t \simeq T_L$, we observe a rather abrupt shift toward a linear dependency in time, consistent with the already noticed saturation of the structure functions and the Lagrangian energy spectra. We know from Figure 7a that $\mathcal{K}$ varies within a factor two in experiments a to f; such a quantitative information is not easily recovered directly from the curves in Figure 8, although it appears roughly consistent with them.

5. The effect of numerical diffusion

a. General considerations. The question of the accuracy of numerical schemes used for simulating particle trajectories has been addressed by Haidvogel (1982) and Haidvogel and Rhines (1983), who show that the first-order forward scheme we have been using here is a scheme of poor quality, according to an efficiency test based on particle conservation of "corrected" vorticity. This test, however, is somewhat inconclusive, for the following reasons. It consists in fact in integrating the Lagrangian vorticity equation along the computed particle trajectory and comparing this Lagran-

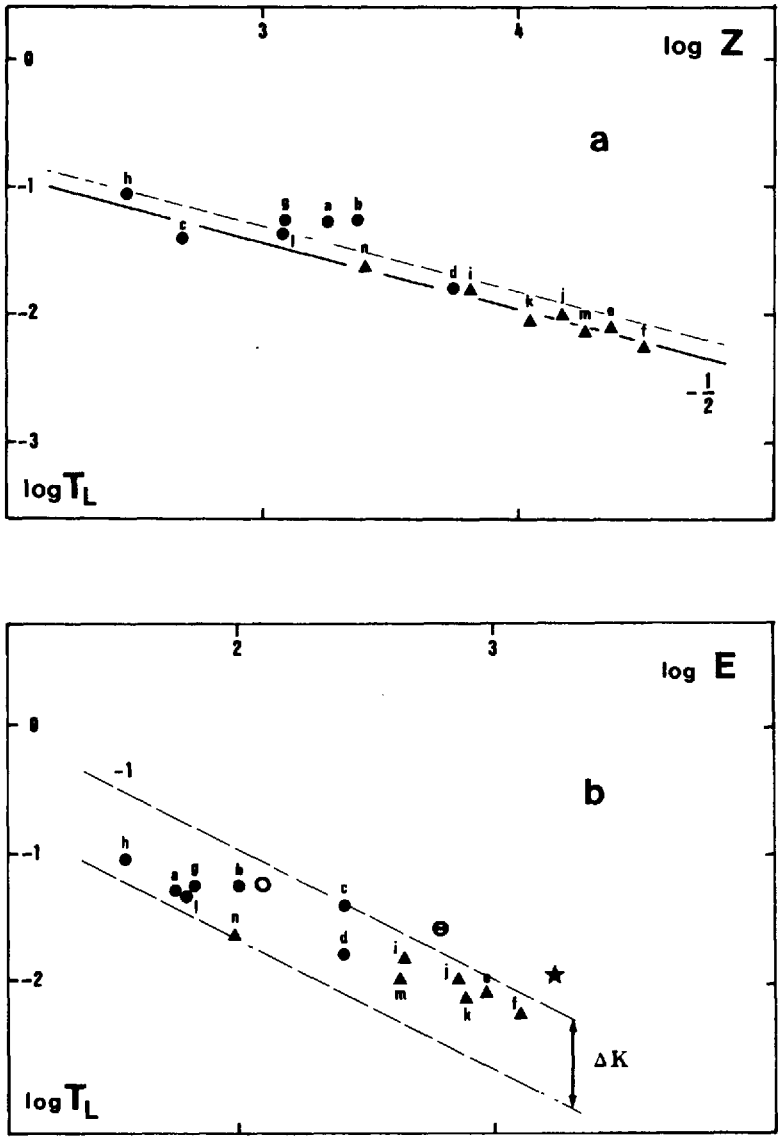

Figure 6. Lagrangian integral time scales T_L versus initial enstrophies (a) and initial energies (b). The symbols ▲ correspond to strongly energetic areas (coherent vortices); symbols ● to weakly energetic areas. In a, the theoretical estimate (17) of T_L is indicated by a discontinuous line; the solid line is a regression line using coherent vortex data only. In b, ⊖ symbol refers to Price's (1981), ○ to Freeland's (1975), and ★ to Colin de Verdière's (1983) measurements.

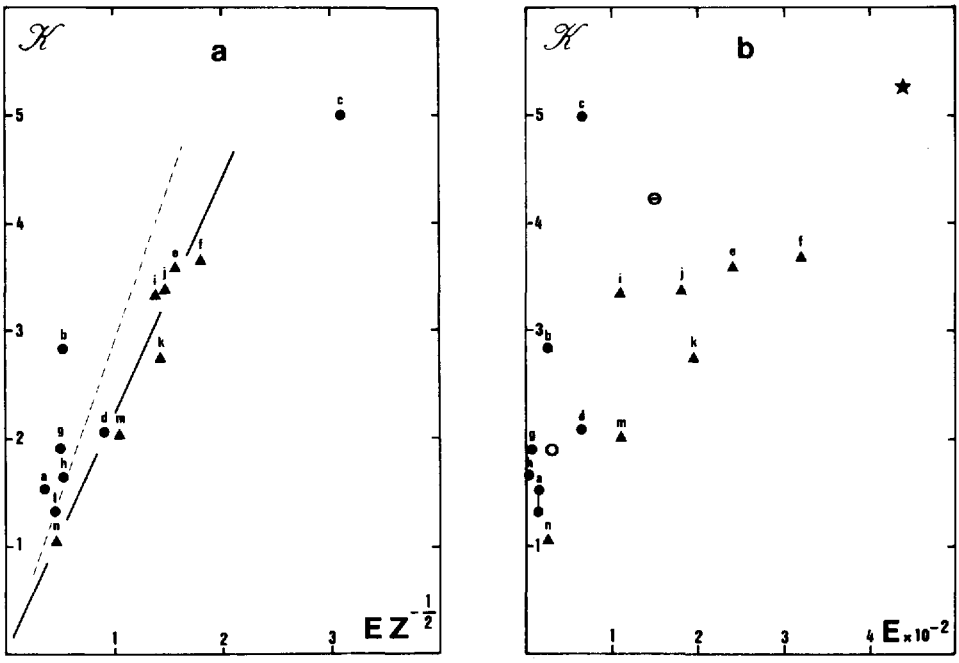

Figure 7. Large-time eddy diffusion coefficient $\mathcal{K}$ versus $EZ^{-1/2}$ (a) and initial energy (b). Same symbols as in Figure 6.

gian prediction with the prediction obtained at the particle location using the Eulerian model. In doing so:

(i) we have to integrate the diffusion term along the trajectory, which introduces an additional source of error;

(ii) the difference between the two values of vorticity at a particle location comes from the numerical errors or uncertainties of both models, due in part to the lack of definition of the sub-grid scales: it is not simply a measure of the Lagrangian model deficiencies;

(iii) even though the initial seed of decorrelation between the two solutions, in terms of Eulerian vs Lagrangian vorticity values, is the difference in truncation errors of the two models, its subsequent growth is actually governed by the local predictability properties of the motion: the lack of continuous dependency on initial data which is characteristic of turbulent flows, makes this test a predictability test rather than an accuracy test.

What we must evaluate is indeed the spurious numerical diffusion induced by our present scheme. We get a first estimation by applying it to a set of particles drifting in a frozen field; such particles would indeed follow the streamline if the displacement

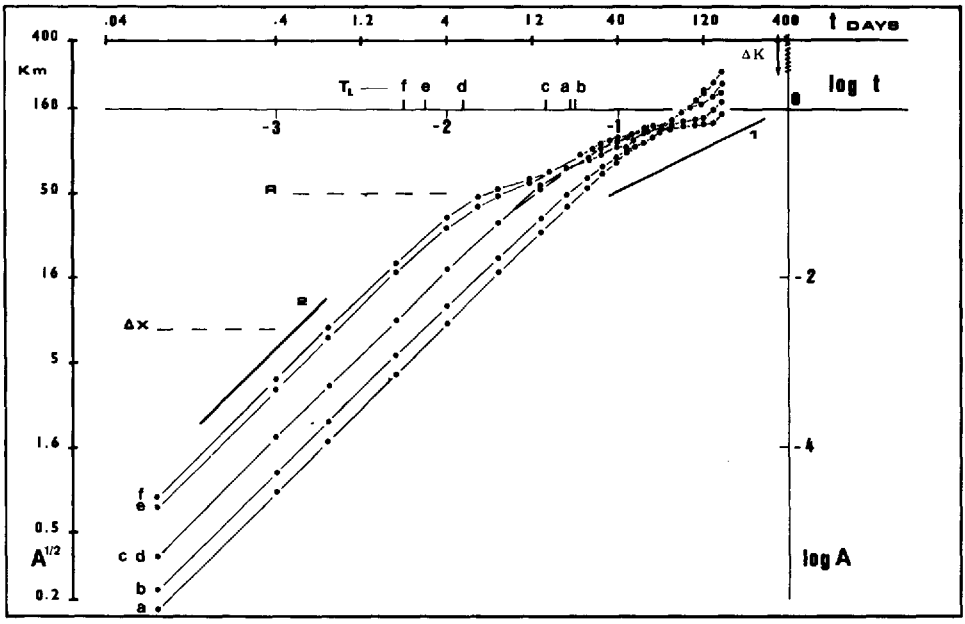

Figure 8. Single-particle dispersions $A(t)$ versus time for the 6 particle sets a to f. The slopes 1 and 2 are indicated, as well as the Lagrangian integral time scale T_L for each set. The mesh size Δx of the numerical model and the forcing scale R are also indicated.

algorithm were exact. We take the frozen field as the motion field at some arbitrary time $t = t_0$; Figure 9 shows the trajectories of five particles followed during 4000 time steps, superimposed on the frozen streamfunction field. On such a time scale we observe rather small departures between trajectories and streamlines, except perhaps around vortices, where particles are slowly expelled from the center.

To get a more quantitative estimate of numerical diffusion, we select six squares $\mathcal{D}_i$ ($i = 1, 6$) of $m \times m$ contiguous gridpoints, chosen to give a fair sampling of the various flow conditions (vortices, active or inactive regions) encountered by a particle in its motion (Fig. 9). For each square $\mathcal{D}_i$ we define a time scale $\theta_i = n_i\tau \simeq 2\Delta x/\sqrt{E_i}$, where E_i is the energy per unit area in $\mathcal{D}_i$; θ_i is thus a multiple of τ which corresponds to an average displacement of roughly two grid intervals for particles belonging to $\mathcal{D}_i$. Then we consider 6 sets of particles which initially coincide with all the gridpoints $\mathbf{a} \in \mathcal{D}_i$, and we move them in the frozen field using $\tau = \Delta t$; we denote by $\mathbf{x}(\mathbf{a}, \theta_i)$ their computed location at time θ_i. The root-mean-square variation of ψ in this motion

$$\Delta\Psi_i^N(\theta_i) = \left(\frac{1}{m^2}\sum_{\mathbf{a}\in\mathcal{D}_i}\{\psi[\mathbf{x}(\mathbf{a}, \theta_i), t_0] - \psi[\mathbf{a}, t_0]\}^2\right)^{1/2} \tag{37}$$

which would vanish for a perfect scheme, is a measure of the spurious numerical

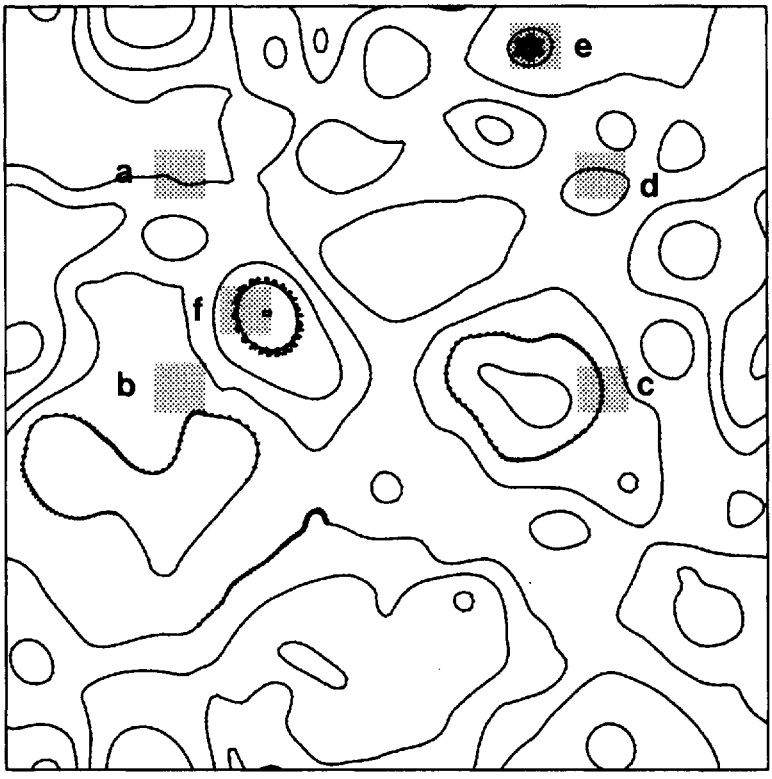

Figure 9. Streamlines of the frozen flow used for testing the particle motion algorithm. Five trajectories lasting over 4000 time steps are shown, together with the six squares $\mathcal{D}_i$ for which the ratio of numerical diffusion to turbulent diffusion is computed.

diffusion for the given flow conditions. Similarly we evaluate the (physical) turbulent diffusion by

$$\Delta\Psi_i^T(\theta_i) = \min_{\alpha\in\mathcal{D}_0}\left(\frac{1}{m^2}\sum_{\mathbf{a}\in\mathcal{D}_i}\{\psi(\mathbf{a}+\alpha, t_0+\theta_i) - \psi(\mathbf{a}, t_0)\}^2\right)^{1/2} \tag{38}$$

where $\mathcal{D}_0$ is the set of translations $(k\Delta x, \ell\Delta x)$, $-m/2 \le k, \ell \le m/2$. Thus (38) is a measure of the deformation of flow structures, the minimum over $\alpha \in \mathcal{D}_0$ being applied to eliminate the local mean motion. The ratios $\Delta\Psi_i^N/\Delta\Psi_i^T$, which measure the ratio of erroneous numerical diffusion to physical diffusion, are displayed in Table 3 for the 6 samples of Figure 9; in (37) and (38) we have taken $m = 10$. Table 3 shows that the effect of numerical diffusion when a time step $\tau = \Delta t$ is used, is roughly an order of magnitude smaller than physical diffusion. The worst case is the vortex f, where we get a ratio of 0.3. The fact that we get a relatively large value there is easy to explain; strong stable vortices tend to induce a relatively large numerical diffusion due to the combined effect of high velocity and curvature, which ejects particles along

Table 3. The effect of numerical diffusion when a time step $\tau = \Delta t$ is used, is roughly an order of magnitude smaller than physical diffusion. The worst case is the vortex f, where we get a ratio of 0.3. The fact that we get a relatively large value there is easy to explain.

Sample $\mathcal{D}_i$	a	b	c	d	e	f
n_i	224	172	108	108	56	49
$\Delta\Psi_i^N/\Delta\Psi_i^T$	0.07	0.06	0.04	0.13	0.14	0.30

spirals; on the other hand, turbulent diffusion there is not particularly large, because the strength of gradients is counterbalanced by stability. Even in this extreme case we find that numerical diffusion is still significantly smaller than turbulent diffusion.

b. Numerical diffusion in a coherent vortex. Let us analyze in more detail the numerical diffusion process within a circular vortex; we choose vortex f, which gave us the worst result in Table 3. Figure 10 shows the Lagrangian correlation $R(t)$ for a

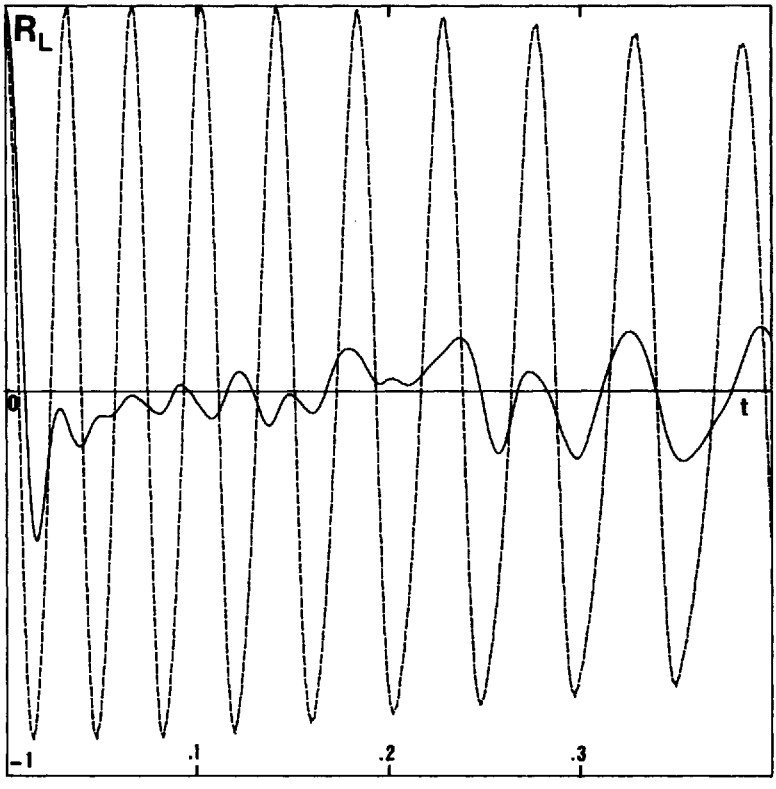

Figure 10. Lagrangian velocity correlation $R_L(t)$ for a single particle released in the frozen vortex f (discontinuous line), compared to the same correlation averaged over 100 particles (solid line).

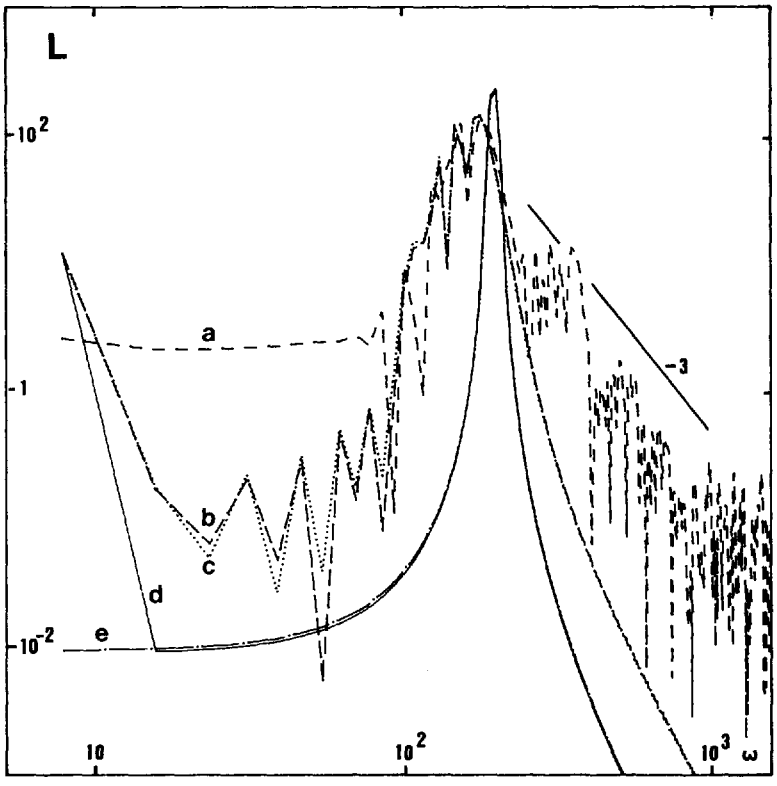

Figure 11. Effect of the numerical diffusion on the Lagrangian energy spectrum (see text for details).

single particle released in the frozen vortex. As expected, $R(t)$ oscillates between 1 and -1, with a period corresponding to one turnaround time. From the beginning however, $R(t)$ does not drop below $-.9$, which means that the path is not a perfectly symmetric curve followed with perfectly regular speed; this has of course nothing to do with numerical diffusion. Numerical diffusion is on the contrary responsible for the long-term trends of the oscillation, characterized by a slow decrease in amplitude and frequency. We thus observe that numerical diffusion begins to affect the correlation significantly after a time of the order of .1; i.e., one order of magnitude above the Lagrangian integral scale $T_L = .0057$.

The effect of this numerical diffusion process on the Lagrangian spectrum can be analyzed on Figure 11, where curve a corresponds to the Fourier transform of the single-particle correlation $R(t)$ of Figure 10; this spectrum is characterized by a broad peak dominating a white noise band at low frequencies, and a ω^{-3} band at high frequencies. The ω^{-3} effect has been already discussed in section 4*b*. Without numerical diffusion we would have obtained something close to a Dirac function

centered at $\omega_R = 2\pi/T_R$, where $T_R = .032$ is the initial turnaround period of the single particle. Numerical diffusion is thus responsible for the broadening of the peak at frequencies $\omega < \omega_R$; this corresponds to the decrease in frequency already observed in Figure 10. To see the effect, on the Lagrangian spectrum, of the various characteristics of $R(t)$, we construct an analytic function

$$\tilde{R}(t) = 2E\left\{\alpha_1 + (1 - \alpha_1)\cos\frac{2\pi t}{T}\exp(-\alpha_2 t^2)\right\} \tag{39}$$

with $T = T_R + t(T_1 - T_R)/T_M$. Here $T_M = .4096$ is the duration of our experiments. Taking $\alpha_1 = .05$, we get for $\tilde{R}(t)$ the observed lower bound $-.9$ of $R(t)$; taking $T_1 = .044$ yields a frequency modulation from an initial period close to T_R, to a final period close to .054 as observed in $R(t)$; and taking $\alpha_2 = 2.22 \times 10^{-7}$ gives us the observed amplitude damping of $R(t)$. With these values of the coefficients, the Fourier transform of (39), performed in the same conditions as for obtaining curve a, yields curve b of Figure 11, which exhibits a similar peak broadening, but misses the low-frequencing white noise. Next, we degrade the approximation by choosing $\alpha_2 = 0$, hereby deleting the amplitude damping (curve c); obviously amplitude damping has little effect on the spectral shape, if we compare curves b and c. We then get curve d by deleting the period modulation, taking $T_1 = T_R$, and curve e by finally setting $\alpha_1 = 0$, thus going back to a perfect cosine curve. The Dirac function centered at $t = T_R$ is well approximated by the two last curves. We conclude from this discussion that most of the spectral peak broadening is due to the frequency modulation associated with numerical diffusion. On the other hand, we have not really explained the low-frequency white noise band; nevertheless, it is reasonable to also attribute it to numerical diffusion, keeping in mind that our simple linear approximation of frequency modulation works well in the immediate vicinity of ω_R (yielding the observed local broadening) but fails to recover the behavior of $L(\omega)$ at very low frequencies.

It is not fortuitous, in fact, that the broadening of a spectral peak associated with single-particle motion within an isolated vortex occurs toward frequencies lower than ω_R. An isolated vortex is a structure where vorticity is maximum at the center and decreases regularly all around. On the other hand, the turnaround period T_R along a closed streamline is easily identified with the average vorticity inside. Therefore, as a particle is steadily expelled away from the vortex center by numerical diffusion, its turnaround period increases.

Figure 12 shows the single-particle dispersion as a function of time, for the case of vortex f. The effect of numerical diffusion is clearly described by the drift of the extrema of curve a, which depicts the evolution of the absolute dispersion of a single tracer released in the frozen vortex. If we compare curve a to curve b, which describes the absolute dispersion of a set of 100 tracers in the same frozen field, we may infer that the contribution of numerical diffusion to absolute dispersion in that case remains negligible as long as t does not reach at least an order of magnitude above T_L.

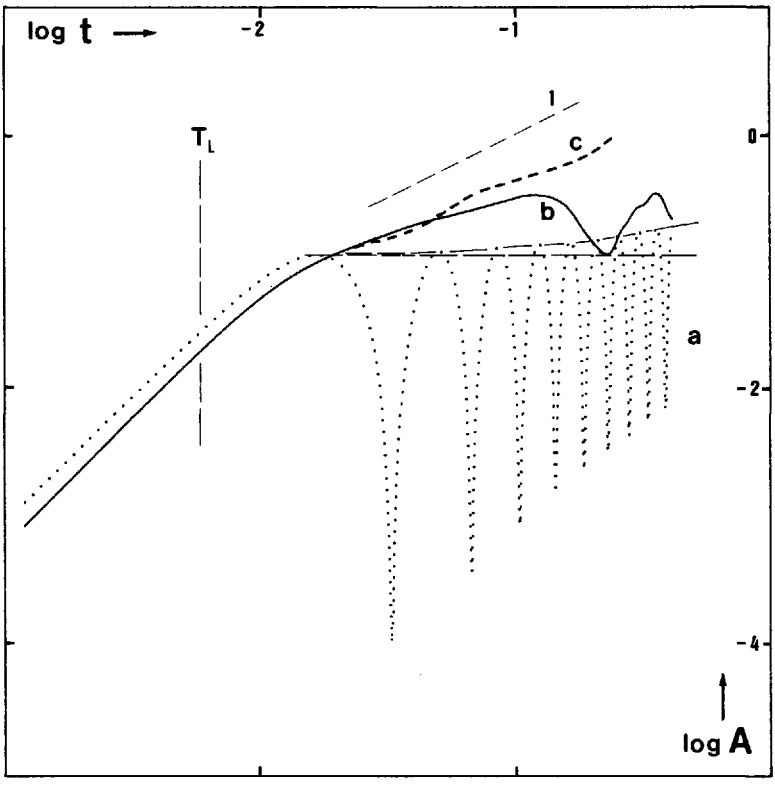

Figure 12. Effect of the numerical diffusion on the single-particle dispersion (see text for details).

c. Evolving fields vs frozen fields. Figure 12 also shows the absolute dispersion of the same initial set of 100 tracers, this time in the evolving vortex f (curve c). Comparing curve c to curve b, we observe that the time evolution of the flow does not alter significantly the absolute dispersion, until times of the order of $10 \times T_L$ are again reached. Of course at very long times, absolute dispersion in a frozen flow domain characterized by closed streamlines becomes stationary or oscillating around a constant value (except for the effect of numerical diffusion which tends to expel particles out of the closed streamline domain), while absolute dispersion in the evolving flow reaches the expected linear dependency of time.

Another illustration of the comparison between frozen and evolving fields is given in Figure 13, which shows the Lagrangian correlation R_L in both cases, for the three patches a, d, f already described (remember that a is a weakly energetic region, d a region with average energy, and f the strongest vortex in the flow). The fact that the flow is frozen or evolving in time has obviously no effect on the Lagrangian time scale.

Thus the fact that the flow varies in time has no significant effect on Lagrangian

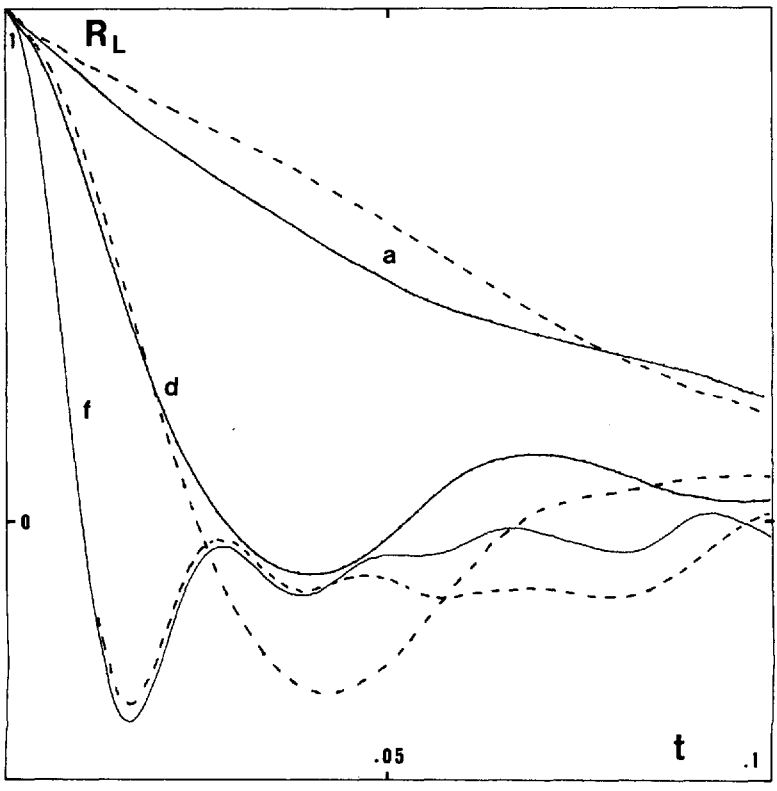

Figure 13. Lagrangian velocity correlations $R_L(t)$ in evolving fields (solid line) and frozen fields (discontinuous line) for particle sets a, d and f.

statistics until we reach time scales $t \gg T_L$. It follows from this that our present statistics are not likely to be influenced by the truncation errors of the Eulerian model in the same range of time scales.

d. Limits of validity of Lagrangian statistics due to numerical diffusion. We may now go back to the discussion of Lagrangian statistics partially developed in Section 4, and evaluate where biases due to numerical diffusion effects might affect the results. Roughly speaking, we may trust everything which deals with time scales not significantly greater than T_L. For example, the frequency shoulders of the Lagrangian energy spectra of Figure 3 are to be trusted. The low-frequency limits of the same spectra, on the contrary, are dubious. We know that $L(\omega)$ must become stationary at very small frequencies, but the fact that stationarity is obtained right from the frequency shoulder might be a numerical diffusion bias; we have seen in Section 5*b* that numerical diffusion tends to broaden spectral peaks toward low frequencies.

Similarly, the estimates of single-particle dispersion shown in Figure 8 are likely to be biased in the large time limit. At very large times, we normally expect, in connection

with the stationarity of $L(\omega)$, an asymptotic linear law (21)

$$A(t) \sim 2\mathcal{K}t,$$

which gives the magnitude of the asymptotic diffusion coefficient $\mathcal{K}$. A direct estimate of $\mathcal{K}$ from Figure 8 is however impossible, because we cannot trust the single-dispersion estimates $A(t)$ in the large-time limit. On the opposite, the estimates of $\mathcal{K}$ given in Figure 7 are reliable, because large time-scales have been discarded in evaluating T_L.

6. Conclusion

The present work confirms the classical asymptotic estimates of single-particle dispersion at small and large times, given by Taylor (1921) and Batchelor (1949). Further, it proves that the classical estimate at small times is more than an asymptotic behavior when the Lagrangian energy spectrum is steeper than ω^{-1}; in that case it is in fact valid all the way up to the integral time scale T_L. For $t < T_L$ and spectra steeper than ω^{-3}, we note a "practical indeterminacy" of the spectral slope, like the one observed in BBS for the Eulerian spectrum, the Lagrangian spectrum, reconstructed from an imperfect set of Lagrangian correlations, tends to saturate at an artificial "background" ω^{-3} slope.

The Lagrangian integral time scale T_L has been related here to the local enstrophy of the flow. This estimate is sustained by the remark that local enstrophy is indeed a Lagrangian invariant in the weak dissipation limit; the relation between T_L and local enstrophy is of course particularly straightforward in the case of a coherent vortex. T_L appears as a very clear boundary between two regimes of the various Lagrangian statistics. As t increases and crosses T_L, single-particle dispersion shifts from a quadratic to a linear dependency of time, the diffusion coefficient reaches its asymptotic value, and the Lagrangian spectrum shifts from a steep power law to a zero slope.

The Lagrangian statistics obtained from numerical experiments at large times ($t \gg T_L$) are difficult to use because they are contaminated by numerical diffusion. The numerical diffusion bias could be alleviated by possibly an order of magnitude, just by using a more elaborate (second order) scheme for extrapolating the particle motion; this has not been done here. It was possible, however, to verify our theoretical prediction of the value of the eddy diffusion coefficient at large times $\mathcal{K} = \sqrt{8\pi/3} \cdot EZ^{-1/2}$, because this value is attained in practice as soon as t reaches T_L. From the present simulations, the experimental estimate of $\mathcal{K}$ was found actually smaller than the theoretical value by 20%; but more recent experiments performed by Lien Hua (private communication) in the barocline case indicate a value 30% higher.

Acknowledgments. The authors are grateful to the unknown referee whose unyielding criticism led to drastic improvement of the paper.

REFERENCES

Babiano, A., C. Basdevant and M. Larchevêque. 1985a. Fonction de structure et spectre lagrangiens d'un écoulement turbulent bidimensionnel. C.R. Acad. Sci. Paris, *300,* 195–198.

Babiano, A., C. Basdevant, B. Legras and R. Sadourny. 1984. Dynamique comparée du tourbillon et d'un scalaire passif en turbulence bi-dimensionnelle incompressible. C.R. Acad. Sci. Paris, *299,* 601–604.

Babiano, A., C. Basdevant and R. Sadourny. 1985b. Structure functions and dispersion laws in two-dimensional turbulence. J. Atmos. Sci., *42,* 942–949.

Basdevant, C., Y. Couder and R. Sadourny. 1984. Vortices and Vortex-Couples in Two-Dimensional Turbulence or Long-Lived Couples are Batchelor's Couples. Lecture Notes in Physics, 230, pp. 327–346.

Basdevant, C., B. Legras R. Sadourny and M. Béland. 1981. A study of Barotropic model flows: Intermittency waves and predictability. J. Atmos. Sci., *38,* 2305–2326.

Basdevant, C. and R. Sadourny. 1983. Modélisation des échelles virtuelles dans la simulation numérique des écoulements turbulents bidimensionnels. J. Mécan. Théor. et Appl. Numéro Spécial, 243–270.

Batchelor, G.K. 1949. Diffusion in a field of homogeneous turbulence. Austr. J. Sci. Res., *A2,* 437–450.

—— 1951. Pressure fluctuations in isotropic turbulence. Proc. Cambr. Phil. Soc., *47,* 359–374.

Bennett, A. F. 1984. Relative dispersion: Local and nonlocal dynamics. J. Atmos. Sci., *41,* 1881–1886.

Colin de Verdière, A. 1983. Lagrangian eddy statistics from surface drifters in the eastern North Atlantic. J. Mar. Res., *41,* 375–398.

Couder, Y., C. Basdevant and H. Thome. 1984. Sur l'apparition de couples solitaires de tourbillons de sillages bidimensionnels turbulents. C. R. Acad. Sci., Paris, *299,* 89–94.

Freeland, H., P. Rhines and T. Rossby. 1975. Statistical observations of the trajectories of neutrally buoyant floats in the North Atlantic. J. Mar. Res., *33,* 383–404.

Frenkiel, F.N. 1952. Application of the statistical theory of turbulent diffusion to micrometeorology, J. Meteor., *9,* 252–259.

—— 1953. Turbulent diffusion: Mean concentration distribution in a flow field of homogeneous turbulence. Adv. Appl. Mech., *3,* 61–107.

Haidvogel, D.B. 1982. On the feasibility of particle tracking in eulerian ocean models. Ocean modelling *45,* 4–9.

Haidvogel, D.B. and P.B. Rhines, 1983. Waves and circulation driven by oscillatory winds in an idealized ocean basin. Geophys. Astrophy. Fluid Dyn., *25,* 1–63.

Holloway, G. and S.S. Kristmannson, 1984. Stirring and transport of tracer fields by geostrophic turbulence. J. Fluid Mech., *141,* 27–50.

Kampé de Fériet, J. 1939. Les fonctions aléatoires stationnaires et la théorie statistique de la turbulence homogène. Ann. Soc. Sci. Bruxelles, *59,* 15–194.

Mc Williams, J. C. 1984. The emergence of isolated coherent vortices in turbulent flow. J. Fluid Mech., *146,* 21–43.

Price, J. 1981. Diffusion statistics computed from SOFAR float trajectories in the western North Atlantic. Unpublished proceedings of CAMS-WHOI Symposium on Lagrangian Tracers. Woods Hole, March, 1981.

Taylor, G.I. 1921. Diffusion by continuous movements. Proc. Lond. Math. Soc., *20,* 196–212.

Received: *10 July, 1985;* revised: *7 October, 1986.*